Directional adhesion for climbing: theoretical and practical considerations

DANIEL SANTOS *, MATTHEW SPENKO, AARON PARNESS,
SANGBAE KIM and MARK CUTKOSKY

Center for Design Research, Stanford University, Stanford, CA 94305-2232, USA

Abstract—Using the gecko as inspiration, important principles are revealed for reliable maneuvering on vertical surfaces. Foremost among these is the directional behavior of the gecko adhesive system, which permits control of adhesion *via* control of the tangential forces at the feet. Multiple hierarchical levels of compliance are also important for conforming intimately to surfaces with varying degrees of roughness and different length scales. In light of these requirements, most previously developed synthetic adhesives are not well suited for application on a climbing robot. We describe a synthetic fibrillar adhesive, termed Directional Polymer Stalks, made from relatively soft polyurethane (modulus of elasticity ≈ 300 kPa). The fibrils are angled 20° with respect to vertical and are approximately 1 mm long and 380 μm in diameter. Rather than having a flat top, they have angled faces at 45°. The directional nature of these angled stalks is shown, achieving a maximum adhesion of approximately 1 N for a 3.9 cm^2 patch when pulled in the direction in which the stalks are angled. When pulled in the non-adhesive direction, the adhesion forces are negligible. The application to a climbing robot is presented and limitations of the current design are discussed along with ongoing efforts to address them.

Keywords: Adhesion; climbing; robot; gecko.

1. INTRODUCTION

Geckos are remarkable climbers and have stimulated research in the fields of adhesion science and robotics to understand and reproduce their adhesion and climbing abilities. They are able to traverse smooth vertical surfaces at speeds of up to 70 cm/s [1] and are also agile climbers on rough and even overhanging surfaces. Geckos attach and detach their sticky feet in about 5 ms and 15 ms, respectively, with negligible preload or pulloff force [1] in the normal direction. Their feet and toes are a hierarchical system of complex structures consisting of lamellae, setae,

---

*To whom correspondence should be addressed. Tel.: 650-723-4258; e-mail: dsantos@stanford.edu

and spatulae. The distinguishing characteristics of the gecko adhesion system have been described in [2] and are listed here: (1) anisotropic attachment, (2) high pulloff force to preload ratio (μ'), (3) low detachment force, (4) material independence, (5) self-cleaning, (6) anti-self sticking and (7) non-sticky default state. Various efforts have been underway to understand and re-create some of these properties in a synthetic adhesive.

Much of the work on reproducing the gecko's adhesive system has focused on creating dry and self-cleaning adhesives. The gecko's adhesive structures are made from β-keratin (modulus of elasticity ≈ 2 GPa) [2]. Such a stiff material is not inherently sticky; however, because of the gecko adhesive's hierarchical nature and extremely small distal features (spatulae are ≈ 200 nm in size), the gecko's foot is able to intimately conform to the surface and generate significant attraction using van der Waals forces.

In the following sections, we examine the gecko adhesion system in order to extract principles that are most critical for the purposes of climbing. We discuss how directionality and conformability, with proper force control from a gecko or robot, can enable robust climbing. We also review a number of adhesives that have been fabricated for a variety of applications. While many of the current synthetic adhesives reproduce various properties of the gecko's adhesive apparatus, they are not ideal for a robot designed to climb like the gecko. In Section 4, a directional synthetic adhesive is presented along with its manufacturing process, detailed performance results and a discussion of its application on a climbing robot. We conclude with a discussion of the limitations of current directional adhesives and ongoing work to overcome them.

## 2. GECKO DIRECTIONAL ADHESION AND IMPLICATIONS

Of the distinguishing characteristics of the gecko adhesion system listed in the previous section, the combination of anisotropic (i.e. directional) adhesion, high μ' and low attachment/detachment forces is particularly useful for climbing. These three characteristics are also coupled — directionality enables a high μ' and low attachment and detachment forces. Low attachment forces are desirable for climbing because the need to apply preload forces in the normal direction at the front limbs of a robot or animal will tend to push it off the wall, causing it to pitch backward. Low detachment forces are also desirable, allowing for less energy expenditure while climbing and reducing force discontinuities and vibrations that can produce slippage. Another beneficial characteristic of the gecko adhesion system is the hierarchy of compliant structures in the toes, lamellae, setae and spatulae that permit conformation to rough surfaces at length scales ranging from centimeters to a few nanometers, ensuring good contact on a wide range of natural surfaces and reliably engaging a high percentage of the spatulae at each step. The gecko's hierarchical structures also serve to reduce the effective stiffness of its adhesive, reducing spring-back forces during contact and increasing adhesion

forces [3]. The gecko additionally uses the compliance of its body and controls forces at its feet to avoid overloading any single region of the contacts between its feet and the surfaces it is climbing. Avoiding local stress concentrations helps to prevent a wave-like peeling that can start in a local area of high contact stress and propagate across the contact patch.

The first studies to show that the gecko adhesive system was directional were adhesion measurements performed on a single seta [4]. A single gecko seta produced over 10 times higher pulloff forces when preloaded in both the perpendicular and parallel directions than just the perpendicular direction. Indeed, it was found that only with a specific 3-dimensional orientation and loading did gecko setae produce significant adhesion forces. The study also showed that over a range of pulloff forces up to 20 µN a single gecko seta always detached at a critical angle of ≈30°. This finding predicts that the loading vector at a foot contact would have to be within 30° of the surface to sustain adhesion forces. Another discussion of the gecko's adhesion directionality [5] looks at the climbing dynamics of the gecko. While climbing, geckos tend to pull all four of their feet inwards toward their center of mass, which may be one mechanism by which the gecko loads its feet in the parallel direction in order to generate adhesion.

Further studies were performed on gecko lamellae (setal arrays) and whole toes. In [6] lamellae were dragged along surfaces with and against their natural curvature while measuring the generated contact forces. When dragged with the natural curvature of the arrays, adhesion was present, but when dragged against the curvature, only friction was observed. Whole toes of the gecko were tested by adhering a single toe of a live gecko to a smooth vertical surface, increasing the angle of the substrate toward overhanging, and then measuring the angle at which the gecko's toe detached from the surface. In these studies, the force vector at the contact (combined perpendicular and parallel forces) during sliding of the lamellae and at detachment of the toes was constant at ≈30°. These results, along with previous results on single seta, have led to a simple empirical model to describe the directionality of the gecko adhesion system. This model, termed 'frictional adhesion', states that the adhesion force is directly proportional to the applied shear load at the contact.

The directional nature of the frictional adhesion model is readily seen in Fig. 1, which shows the model in force–space and describes the sustainable forces at the contact interface before failure by either sliding or pulloff. When loaded in the adhesive direction, adhesion forces can be sustained in proportion to the tangential load applied. When loaded in the opposite direction, Coulomb friction is observed. An upper limit is imposed on the shear load that can be applied, which is a function of the substrate strength, limb strength and adhesive strength. Currently, the exact nature of the gecko adhesive system at higher shear loads is unknown and so this arbitrary limit is expected to be conservative. Mathematically, the frictional
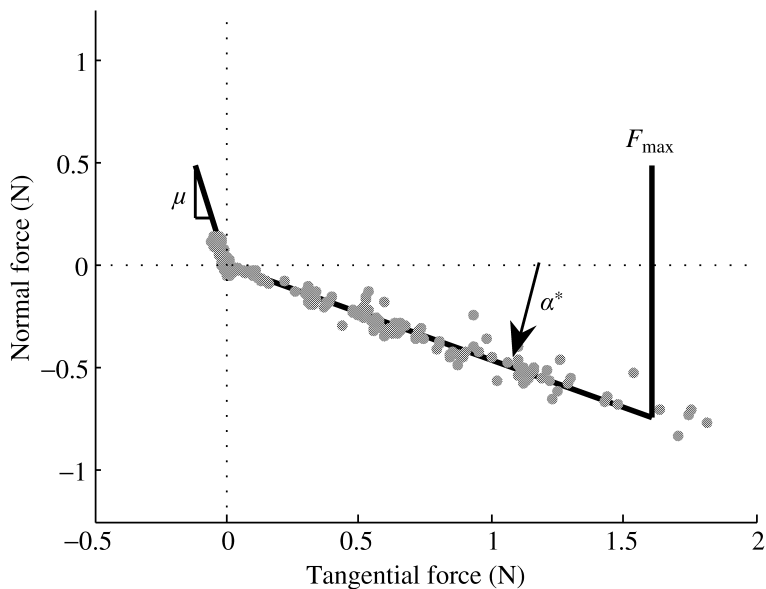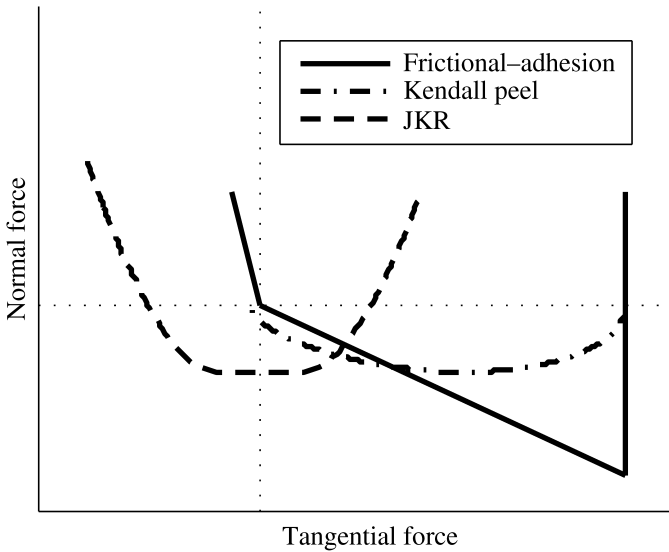
Figure 1. Frictional adhesion model in force–space given in [6]. Data points are from [4, 6] for gecko setae, lamellae and toes. In the adhesion direction (positive tangential), adhesion force is directly proportional to applied tangential force. This line is described by the angle α^*. In the negative tangential direction, Coulomb friction is observed and is described by the coefficient of friction, μ. An arbitrary upper limit ($F_{\max}$) is imposed on the amount of tangential force that can be applied, taken to be a function of material, contact and limb strength.

adhesion model is described by the following set of equations:

$$
\begin{aligned}
F_N &\geqslant -\frac{1}{\mu} F_T \\
F_N &\geqslant -\tan(\alpha^*) F_T
\end{aligned}
\quad
\begin{cases}
F_T < 0 \\
0 \leqslant F_T \leqslant F_{\max}.
\end{cases}
\tag{1}
$$

F_N is the normal (perpendicular) force, F_T is the tangential (parallel or shear) force, μ is the coefficient of friction, α^* is the critical angle and $F_{\max}$ is the maximum limit on tangential force. Data from [4, 6] for setae, lamellae, and whole toes are also plotted in Fig. 1, representing the maximum forces at the time of pulloff and forces sustained during sliding, both of which characterize the forces that the contact can sustain without failure. The $F_{\max}$ limit is chosen to roughly correspond to the highest observed shear loads that follow a linear relationship with adhesion.

The frictional adhesion model captures the three features of the gecko adhesive system that arise from directionality. Anisotropic attachment is achieved simply because frictional adhesion only exhibits adhesion when there is a positive tangential force, corresponding to the preferred loading direction. Frictional adhesion can also achieve a high value of μ' because normal pulloff force is not a function of the applied normal preload force (in practice, a small preload force is needed to establish initial contact; however, the applied tangential force then aligns the setae and brings large numbers of spatulae into contact). Low detachment force also follows from

Figure 2. Comparison of three adhesion contact models. The Johnson–Kendall–Roberts (JKR) [7] model is for a spherical elastic asperity in contact with a flat substrate. The Kendall model [8] is for thin-film peeling. The frictional–adhesion model is based on experimental results for the gecko adhesion system [6]. The models have been scaled to show qualitative differences in behavior.

the model — it suffices to relax the applied tangential force, thereby moving toward the origin in Fig. 1. In summary, the frictional adhesion model describes a controllable adhesion system: adhesion in the normal direction is controlled indirectly by controlling the applied tangential force.

Further insight into the implications of the frictional adhesion model is obtained by comparing it directly with two well-known adhesion models from the literature, as illustrated in Fig. 2. Numerical values for the models have been adjusted to give an approximately equal maximum pulloff force in each case. For each model, combinations of normal and tangential forces above the corresponding curve are 'safe' and will not cause the contact to fail by pulloff or slippage. The Johnson–Kendall–Roberts (JKR) model [7] describes the adhesion behavior of a spherical elastic solid in contact with a flat surface. As expected, it is not directional. Moreover, the maximum adhesion force is obtained when there is zero applied tangential force. In contrast, the Kendall tape peel model [8] is directional and qualitatively similar to the frictional adhesion model; pulling nearly tangential to the surface results in higher peel forces than pulling perpendicular to the surface. However, the Kendall model describes the behavior of an adhesive film, which generally requires an initial preload for attachment and peels at a certain speed when pulled. As discussed in [6], each of these models results in different strategies for adjusting the normal and tangential forces at the feet of a climbing robot or animal on sloping, vertical or overhanging surfaces. For example, the frictional adhesion

model suggests that a gecko descending head-first should reorient its rear feet to be facing backwards, which is consistent with observations of geckos.

Thus far we have considered forces in a single plane containing normal and tangential force components, where the normal direction is perpendicular to the surface and the tangential direction is aligned with the gecko's toes, running from the proximal to the distal ends. Geckos also apply some forces in the lateral direction, which is orthogonal to the normal-tangential plane; however, the adhesion effects of loading in the lateral direction have not been reported. It is also important to consider how the limb and whole body dynamics of the gecko work with the feet and toes to produce agile climbing. It would be useful to measure the different foot orientations of geckos on level, vertical, and overhanging surfaces and to correlate these measurements with whole body and individual foot contact forces during climbing. Such results would provide another test of predictions derived from directionality and the frictional adhesion model.

3. GECKO-INSPIRED ADHESIVES: CURRENT STATUS AND REQUIREMENTS FOR VERTICAL SURFACE MOBILITY

Examples of synthetic adhesives comprised of stalks made from materials such as polyurethane, silicone rubber or carbon nanotubes can be found in [9–19]. These efforts have begun to produce promising levels of adhesion and resistance to contamination. The variety of manufacturing solutions is partially a result of the array of potential applications, which include electronic circuit manufacturing, medical surgery and climbing robots.

Although most of the applications would probably benefit from all of the features of gecko adhesives as described in Section 1, the importance of these features varies. For example, as mentioned in the previous section, a climbing robot requires two aspects of a gecko-like adhesive: (1) directionality that allows low attachment and detachment forces, an ability to increase adhesion by increasing tangential force, and a high μ' and (2) a compliance hierarchy that ensures a sufficient proportion of the adhesive material interacts with the climbing substrate on rough surfaces. The ability to be impervious to fouling is also desirable in a climbing robot, but not essential for short distances and clean substrates or as long as the patches can be easily cleaned.

There have been several previous efforts to create robots that climb as well as geckos. A wall-climbing robot that uses a gecko-inspired micro-structured tape [16] has been demonstrated [20] and is able to climb vertical smooth surfaces. Another robot has been developed [21] that uses soft elastomeric pads for climbing and is able to climb surfaces up to 85°. Both of these robots have furthered the development of robust wall-climbing robots; however, neither was able to reproduce the gecko's ability to easily and quickly attach and detach its adhesive feet. In the second case it was noted that speed was limited due to vibrations caused by attachment and detachment.
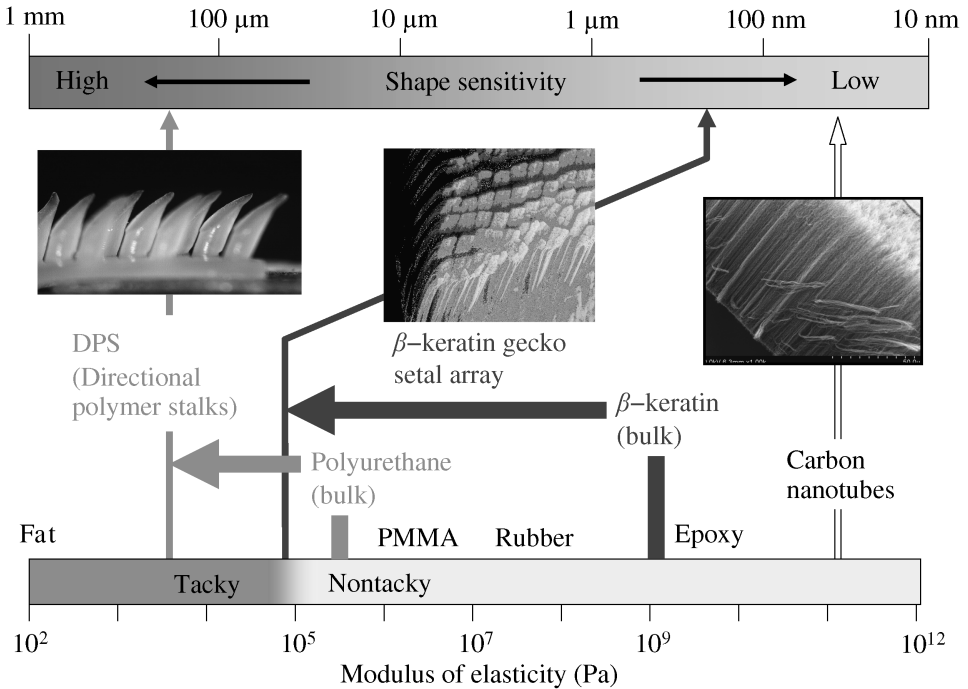
Figure 3. Relationship between modulus of elasticity and sensitivity to tip geometry. Materials that have a higher modulus of elasticity such as carbon nanotubes are more impervious to dirt and more insensitive to the tip geometry; however they must employ a more complex compliance hierarchy to ensure proper contact with the substrate. Values for the stiffness of β-keratin and the effective stiffness of the gecko adhesion system are from [22].

To properly duplicate the climbing ability of the gecko, it is important to understand the relationship among the material's modulus of elasticity, feature size and feature geometry. These properties are shown for some examples of adhesive structures in Fig. 3. As mentioned in Section 1, the gecko's β-keratin is stiff in its bulk state, which gives the gecko its ability to resist dirt. However, because of the gecko's compliance hierarchy, the foot structure acts as if it were below the Dahlquist Tack Criterion (modulus of elasticity less than 100 kPa) [22, 23] and becomes a tacky surface. In general, as the modulus of elasticity increases the adhesive will become less prone to fouling by dirt, but will require a more complex compliance hierarchy to ensure proper contact with the surface. For extremely small elements such as carbon nanotubes, the shape sensitivity (Fig. 3 top) is low, but for softer materials and larger features (on the order of 100 μm) tip geometry dramatically affects adhesion. At these sizes, the optimal tip geometry, where stress is uniformly distributed along the contact area, has a theoretical pulloff force of more than 50–100 times that of a poor tip geometry [24]. Many researchers have attempted to mimic the resistance to dirt by creating very small structures out of stiff materials such as carbon nanotubes or polypropylene [19]. Other solutions,

including the one presented in this paper, have used larger features coupled with softer materials such as polyurethane or poly(vinylsiloxane) [14, 16], which reduces the complexity of the required compliance hierarchy. Here we highlight several of the solutions with an emphasis on the variety of design and manufacturing techniques.

One of the earliest attempts at creating small fibrillar structures for adhesion used an electron-beam lithography process followed by dry etching in oxygen plasma to create structures with diameters between 0.2 and 4 µm and heights ranging from 0.15 to 2 µm [10]. Adhesion was validated using an atomic force microscope (AFM) in contact with a small number of the hairs. However, this is not a practical measurement for the larger sample sizes required by a climbing robot. A larger patch size on the order of hundreds of square millimeters did demonstrate adhesion when coupled with a soft backing; however, the stiff hairs broke off after a few attachment/detachment cycles.

Another approach used multi-walled carbon nanotubes (MWCNTs) to create dry adhesion [18]. The 10–20 nm diameter and 40 nm long MWCNTs were deposited on silicon substrates. The top 25 µm were etched such that the tips were at an even height. This allowed the researchers to bypass the need for a compliance hierarchy when adhering to smooth surfaces such as glass; however, the lack of compliance hierarchy makes this solution impractical for a climbing robot.

In contrast to the research that is focused on the resistance to fouling, there is a body of work focused on creating adhesives using softer materials (although still with a modulus of elasticity higher than the tack criterion). One adhesive was created by pouring poly(vinylsiloxane) into a mold to create a large number of hexagonal patterned stalks [11, 25]. The stalks are 100 µm tall and have a narrow neck joint with a thin plate-shaped head that has a larger diameter than the rest of the stalk. The diameter of the stalks varies from 60 to 20 µm. 2.9 mm diameter patches of the material adhered well to smooth glass with a pulloff force between 350 and 400 mN with preload values between 50 and 130 mN. The material did become dirty over time but regained its adhesive properties when washed.

A similar geometry was obtained by [14] using a polyurethane elastomer with feature sizes around 4.5 µm in diameter and with a 9 µm tip diameter. The structures were 20 µm in length and achieved up to a 400% increase in adhesion compared to the bulk material.

One other application of note is made using MEMS techniques [15, 26, 27]. A silicon dioxide platform is covered with polymeric nanorods that are approximately 250 nm in diameter and 4 µm high. These nanorods are supported by a silicon pillar that provides an additional level of compliance. Using these structures the researchers were able to generate about 20 Pa of adhesion pressure. However, since the adhesion is only measured in the normal direction it would not be suitable for a climbing robot that also needs to sustain force in the tangential direction.

Finally, recent work has emerged that uses a photoresist to create molds out of silicone rubber [28]. Different polyurethanes were poured into the molds to create

both vertically oriented and angled stalks ($\approx 20°$). Stalk diameters varied between 17–25 μm and lengths varied between 30–100 μm. These fibrillar arrays exhibited a maximum adhesion of about 18 mN when tested with an 18 mm diameter glass hemisphere. Although fibrils were angled in these samples, results were only shown for tests along the normal axis.

A comparison of several representative examples of synthetic adhesives is shown in Table 1. The last column refers to the directional polymer stalks presented in Section 4 of this paper. For practical use in a robot that climbs windows and other smooth surfaces, a subset of the required characteristics is listed below, assuming a small robot with a mass of ≈ 0.15 kg, a center of mass ≈ 1 cm away from the surface, a bodylength of ≈ 10 cm and a maximum practical foot size of 3 cm^2/foot:

- Typical pulloff forces $\geqslant 0.1$ N/cm^2.

- Shear forces $\geqslant 0.5$ N/cm^2.

- Maximum preload forces of no more than 0.02 N/cm^2 to prevent the robot from pushing itself off the wall. Some previous adhesive climbing robots have circumvented this limitation with a clever spoked-wheel design that allows the detachment force at a receding point of contact to provide the necessary attachment force at the next contact [29]; however, this method still results in inefficient energy expenditure.

- Negligible detachment forces to prevent vibrations and slippage and to reduce unproductive expenditure of energy.

- Fabricated patch areas of 2 mm^2 or greater that can be tiled and assembled to the underside of a robot foot.

- The ability to survive thousands of attachment/detachment cycles without degradation.

- The ability to operate for several minutes on windows and similar surfaces without becoming completely fouled (the actual life will of course depend on how dirty surfaces are and with what they are contaminated).

As Table 1 reveals, each of the approaches has certain advantages. For example, the adhesives made from stiffer materials and smaller feature sizes have the potential to resist fouling with dirt particles. The structures made from softer materials can ease manufacturing effort by utilizing larger feature sizes while still achieving useful levels of adhesion and friction. However, as the feature size increases, the shape sensitivity of the tips also increases, requiring more complicated distal geometries. None of the solutions achieves all of the desirable characteristics of the gecko and, with the exception of the directional polymer stalks, none has demonstrated the desired directional frictional adhesion behavior.

Table 1.

A comparison of several representative examples of different technological approaches to synthetic dry adhesives in terms of features and functional capabilities relevant for a climbing robot. Values for μ' are given with the corresponding adhesion pressure shown in parentheses at which they are calculated

	Gecko [2, 4, 5]	Geim [10]	Yurdum-akan [18]	Gorb [11]	Kim [14]	Northen [26]	DPS (this work)
Material	β-Keratin	Polyimide	Carbon nanotubes	Poly(viynl siloxane)	Poly-urethane	Polymer nanorods	Poly-urethane
Bulk modulus of elasticity (GPa)	1–3	3	600–1000	0.003	0.003	Not given	0.0003
Feature diameter (μm)	0.2	0.5	0.05	40	9	0.2	380
Feature length (μm)	30–130	2	40	100	20	3	1000
Tested patch size (mm²)	≈10 (one toe)	100	3E-10	6.6	225	25	400
Maximum adhesion pressure (kPa)	100	30	Not applicable due to small sample test area	60	180	0.017	2.4
μ' (at kPa)	8–16	0.06 (30)		7.5 (55)	1.5 (180)	0.3 (0.017)	13 (2.25)
Dirt resistant	Yes	Likely	Likely	No	No	Likely	No
Directional	Yes	No	No	No	No	No	Yes
Levels of hierarchical compliance	3	1	1	1	1	2	1

# 4. A SYNTHETIC DIRECTIONAL ADHESIVE FOR A CLIMBING ROBOT

4.1. Design and manufacturing of directional polymer stalks

In this section we present a synthetic adhesive consisting of directional polymer stalks (DPS) that reproduces the anisotropic nature of the gecko's adhesive system. Like other synthetic dry adhesives, the DPS consist of arrays of features that interact with a surface to produce adhesion *via* van der Waals forces. The directional behavior of the DPS arises from their geometry, which is inspired by the angled, curved shapes of gecko setae. In order to use readily available manufacturing processes, some trade-offs were necessary to achieve the desired geometry. Consequently, the current generation of DPS has considerably larger feature sizes than gecko setae and most of the synthetic adhesives reviewed in Section 3. As discussed in Section 3, there is a relationship between feature size and material stiffness that must be followed in order for the structure to conform intimately to the substrate. Due to the larger feature sizes of the DPS, a soft elastomeric material is used, with a Young's modulus of $E \approx 300$ kPa. These design choices sacrifice long-term durability and the ability to resist fouling for directional adhesion performance on smooth surfaces.

The geometry of the DPS is shown in Fig. 4. Stalks are 1 mm long from base to tip and 380 μm in diameter, extending from a layer of bulk material that is approximately 250 μm thick. The stalks are angled at 20° and the stalk faces are angled at 45° with respect to the vertical. They are arranged in a hexagonal pattern for maximum stalk density and their centers are spaced apart by 1 mm. The DPS are manufactured in patches that are eventually used as toes of a climbing robot. Each
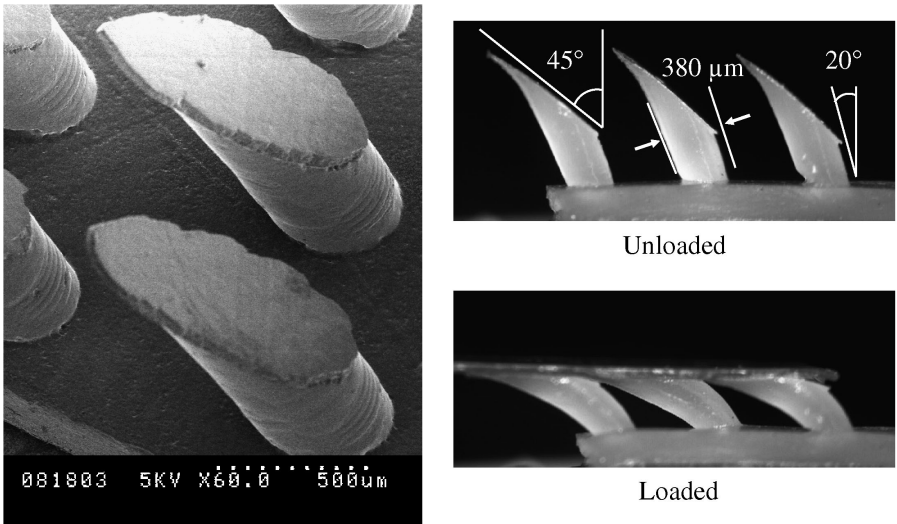
Figure 4. SEM micrograph (left) and side views of DPS geometry (right) in both the unloaded and loaded states. Stalks are 380 μm in diameter and about 1 mm long. Stalk faces are angled 45° and stalks themselves are angled 20° with respect to vertical. Tips of the DPS are <30 μm thick.
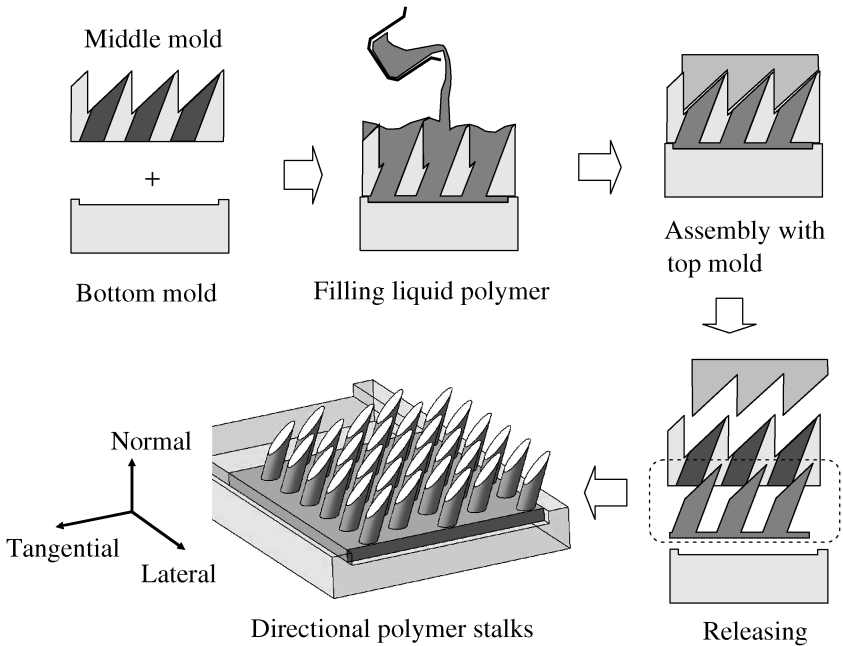
Figure 5. Schematic description of the DPS manufacturing process. Liquid polymer is molded to create proper DPS geometry and mold is disassembled to remove DPS patches. Axes provided to name and distinguish different directions of the angled DPS.

patch is about 3.9 cm^2 in area and roughly elliptical in shape, containing about 500 angled stalks. Final geometry of the DPS was arrived at through experimentation. Stalk diameter was limited by available drill sizes and other parameters were limited by ease of manufacturability.

The DPS are created by casting a liquid polyurethane (Innovative Polymers, Saint Johns, MI, USA; IE-20 AH Polyurethane, Shore-A hardness 20, modulus of elasticity $\approx$ 300 kPa) into a mold (Fig. 5). The mold used to create the DPS is comprised of three parts. The middle mold is created from 1.6 mm thick Delrin (DuPont, Wilmington, DE, USA), which has low surface energy so that it does not bond to the curing polymer. First, V-shaped grooves are cut into the Delrin using a custom slitting saw with a 45° bevel. A silicone rubber (TAP Plastics, Mountain View, CA, USA; Silicone RTV Fast Cure Mold-Making Compound) is cast on top of the middle mold to create a well-matched top mold. Holes are then drilled at 20° on the 45° faces left from the previous cutting operation, completing the middle mold. The bottom mold is made from hard wax to create the proper patch shape for use as a toe on a climbing robot.

The bottom and middle molds are assembled and then liquid polymer is poured into the mold. The top mold is then applied and squeezes any excess polymer out the sides of the fully-assembled mold. The polyurethane then cures and the DPS are released by disassembling the mold. An alternative molding process not involving

a top mold has also been used. In this process, excess polymer is simply wiped away and the tips of the DPS are allowed to cure while exposed to atmospheric moisture, which results in a softer cured product. This process creates stickier tips; however, results are less repeatable due to variations in ambient humidity and in the wiping process. Consequently, specimens from the first process were used for all tests reported in the next section.

4.2. Adhesion testing and results

Previous investigations of synthetic adhesives have generally involved preloading samples against a substrate and then pulling them off, applying force purely along the normal direction. This results in a 1-dimensional characterization of adhesion. To study directionality, it is necessary to explore how motions in the two directions referred to here as the tangential and lateral directions (Fig. 5) affect adhesion pulloff forces. In order to analyze the DPS, a 3-dimensional characterization of adhesion is required.

A 3-axis positioning stage (Velmex, Bloomfield, NY, USA; Part #s MAXY4009 W2S4, MA2506B-S2.5) was used to move patch samples along controlled trajectories with a position tracking accuracy of ± 25 μm. The patches were brought into contact with various substrates affixed to a 6-axis force/torque sensor (ATI Industrial Automation, Apex, NC, USA; Gamma Transducer SI-32-2.5) with a measurement accuracy of ± 25 mN. The force/torque sensor was mounted on a 2-axis alignment stage (Newport Corporation, Irvine, CA, USA; 30 Series Tilt Platform, Model 39) used to align the sample to the substrate. Alignment is performed by manually adjusting two control knobs on the alignment stage and visually inspecting the sample and substrate. The positioning stage was controlled with custom electronics and software. The entire system interfaced with a PC running LabView (National Instruments, Austin, TX, USA) that sampled position data at 500 Hz and force/torque data at 1 kHz. The forces throughout a contact experiment and subsequent pulloff were analyzed using Matlab (The Mathworks, Natick, MA, USA). Because of the complicated geometry of the DPS, the directions of the pulloff and/or sliding forces were not necessarily aligned with the direction of velocity of the sample. In all experiments, the time of contact failure, either by separation of the sample from the substrate or by sliding of the sample along the substrate, was defined as the time at which the dot product between the force vector and the velocity vector was maximum. This method is based on a maximum power principle [30] and pulloff forces were determined by using the measured forces at the time of failure. In most instances, this method recorded pulloff forces when the normal adhesion force was maximum, but in cases where sliding initiated before separation, pulloff forces were recorded when lateral and tangential forces were maximum.

4.2.1. Directionality of the DPS. The first tests performed on the DPS were similar to the tests performed on single gecko seta and arrays of setae [4, 6] specifically looking at the normal and tangential characteristics of the DPS. Samples
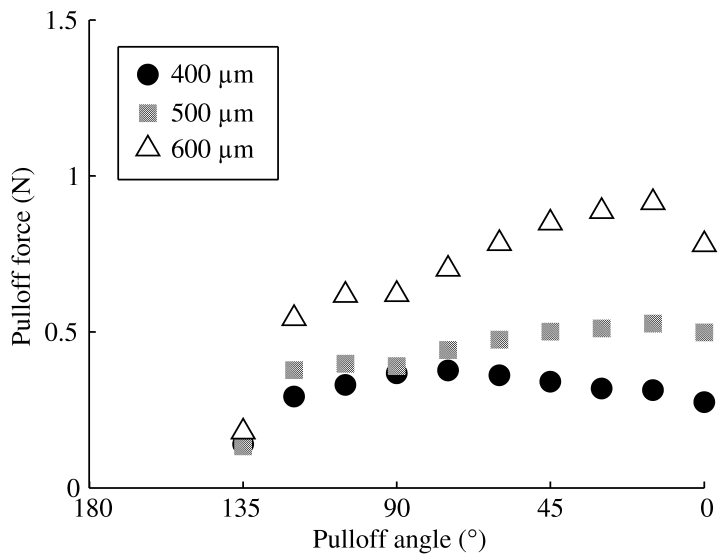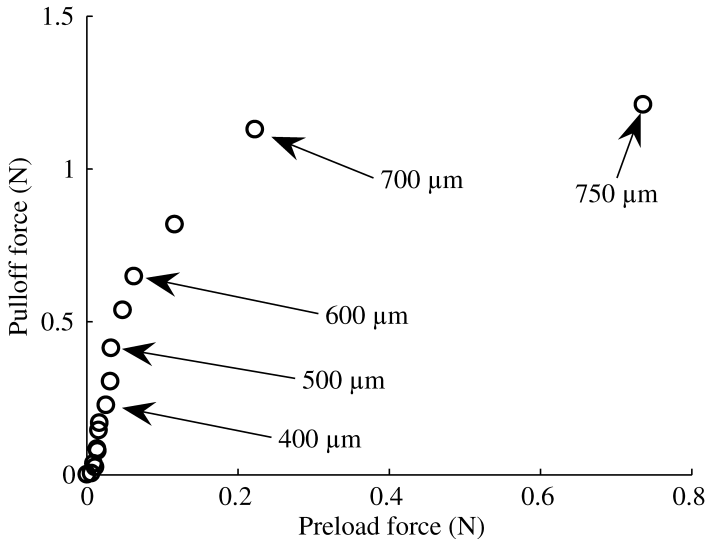
Figure 6. Pulloff forces of 3.9 cm^2 DPS patches as a function of pulloff angle. Patches were moved in the normal and tangential directions only. The positive tangential direction (adhesion direction) corresponds to 0°, the positive normal direction corresponds to 90°, and the negative tangential direction corresponds to 180°. Three different preload depths are given to show dependence of maximum adhesion on initial preload. Data show that adhesion force is present and increases when pulling in the positive tangential direction. No adhesion is present when pulling in the non-preferred (negative tangential) direction.

were brought into contact along a 45° trajectory with a flat glass substrate and preloaded to a specified depth in the normal direction. The samples were then pulled away from the glass at angles ranging between 0° and 180°, where 0° corresponds to dragging the samples with the angle of the stalks (i.e. preferred direction for adhesion) and 180° corresponds to dragging the samples against the angle of the stalks. Speed was held constant across all tests at 1 mm/s, chosen empirically as a trade-off between increasing the speed to minimize the duration of each test and decreasing the speed to minimize viscoelastic effects caused by the polyurethane material. The forces at either pulloff from the substrate or the onset of sliding were recorded to determine maximum adhesion force.

The results from these tests are shown in Fig. 6 for a number of different preload depths. The data in Fig. 6 are for one full patch of the DPS, with an area of 3.9 cm^2 containing ≈500 individual stalks. The results clearly show that the DPS exhibit a directional property. When the DPS are pulled in the direction aligned with the stalk angle, they exhibit adhesion; when they are pulled against the stalk angle, adhesion reduces and eventually no adhesion is present. Pulloff angles above 135° resulted in no measurable adhesion forces because sliding and/or stalk buckling occurred before final pulloff was achieved. The DPS exhibit maximum adhesion at pulloff angles from 15°–30°. The maximum pulloff force over all of these tests was 0.9 N, corresponding to a preload depth of 600 μm.

4.2.2. Effect of preload. The effects of different preloads were examined to determine what range of preload would produce maximum adhesion. Figure 7 shows how pulloff forces were affected by the preload force and depth applied to the sample. All results in Fig. 7 are for a pulloff angle of 30°, which was previously determined to produce high levels of adhesion. Higher preload depths increase the maximum amount of adhesion sustained by the DPS up to a saturation point, occurring at ≈700 μm. At this point, higher preloads may actually cause less adhesion because the stalks buckle and deform such that the stalk faces are no longer making good contact with the substrate.

4.2.3. Work of adhesion and μ'. From these experiments, two other adhesive properties can also be analyzed, namely the ratio of normal pulloff force to normal preload force, μ', and the work of adhesion, W_{adh} [31]. It is known that geckos achieve a μ' between 8 and 16, depending on loading [2]. Figure 8 shows the μ' achieved by the DPS at different pulloff angles. Because the DPS are directional, μ' is not a single value but varies depending on how the DPS are loaded. Figure 8 shows that under the proper loading conditions the DPS can achieve a μ' of up to 13. The figure also shows that, not surprisingly, μ' is controllable since pulloff force is controllable, because for a given preload depth the preload force is roughly constant. Values for μ' at pulloff angles above 135° are not shown because, as discussed previously, no adhesion was measured at these pulloff angles. In Fig. 9, the work of adhesion at different pulloff angles is shown. The work of adhesion is the work loop performed by the sample from when it is first brought into contact

Figure 7. Pulloff forces of 3.9 cm^2 DPS patches as a function of the initial preload force in the normal direction. Data shown for a pulloff angle of 30° in the normal-tangential plane and for preload depths between 0 and 750 μm in 50 μm increments. Pulloff force initially increases with increasing preload force, but begins to saturate at a preload depth of 700 μm.
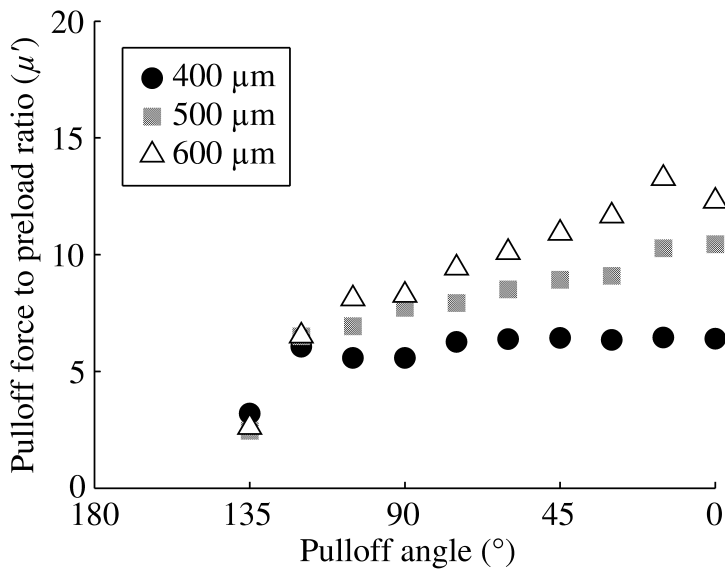
Figure 8. Ratio of the normal pulloff force to the normal preload force (μ') of the DPS patches as a function of pulloff angle. The same trend is present for μ' as for the pulloff force because, for a given preload depth, preload force was relatively constant. Data are shown for preload depths of 400 μm, 500 μm and 600 μm. DPS patches exhibited a μ' as high as 13 when also producing an adhesion force close to 1 N over the 3.9 cm^2 patch.

until it is separated from the substrate [31]. It can be calculated numerically by summing (integrating) the dot product of the force vector and the displacement vector at each time step of sampled data. The work of adhesion is not shown for pulloff angles of 0° or 180° since the samples do not separate in these cases but begin to slide against each other instead. The maximum work of adhesion achieved by the DPS was 2.5 J/m^2, for a pulloff angle of 15° and a preload depth of 600 μm. The ratio between the maximum and minimum work of adhesion, for a preload depth of 600 μm, was greater than 13.

4.2.4. Three-dimensional tests. To further explore the adhesive nature of the DPS, 3-dimensional pulloff tests were performed. In these tests, samples were again preloaded to a specified depth in the normal direction along an approach trajectory of 45°. Again, speed was held constant at 1 mm/s. Here, instead of pulling samples away from the substrate only along vectors in the normal-tangential plane, samples were pulled away from the substrate in all three directions, normal, tangential and lateral. From these tests, the pulloff forces can be plotted in 3-dimensional force-space to determine what the force limits of the contact are before pulloff or sliding occurs.

Figure 10 shows the results from these tests in only the normal-tangential plane. The data are the normal forces (negative values represent adhesion and positive values represent compression) and tangential forces at pulloff or at the onset of
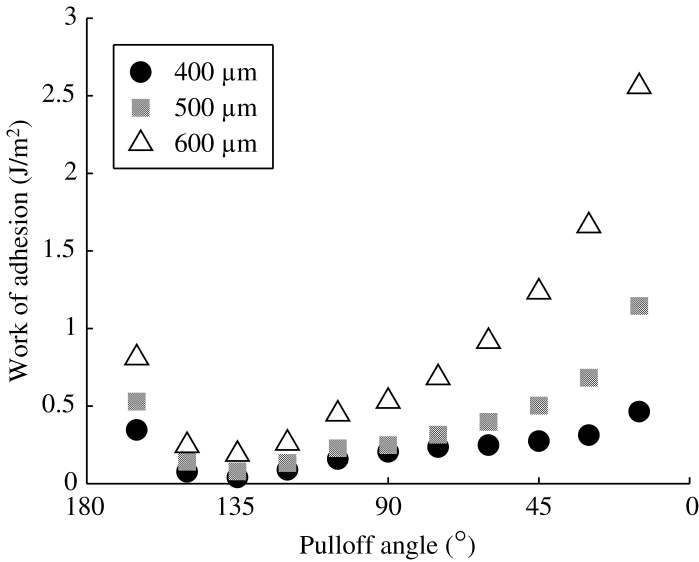
Figure 9. Work of adhesion of the DPS patches as a function of pulloff angle. Data show a large range of values depending on the pulloff angle. Ratio between maximum work of adhesion, at 15°, and minimum work of adhesion, at 135° was greater than 13 at a preload depth of 600 μm.
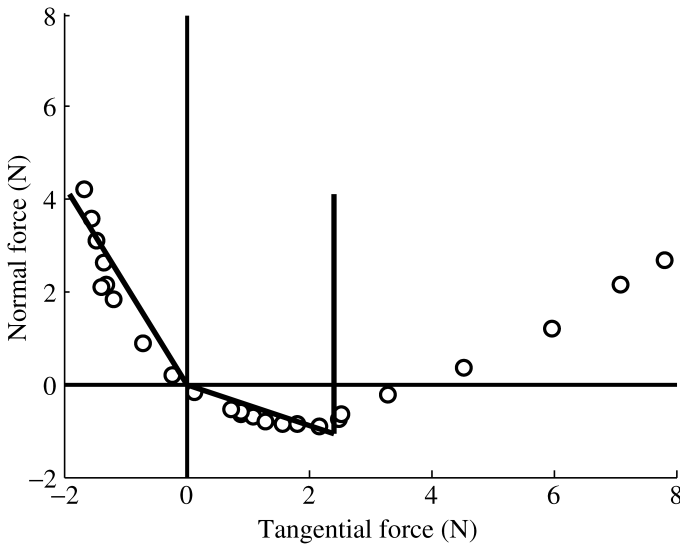

Figure 10. Contact failure forces (shown as circles in the figure) of the 3.9 cm^2 DPS patches in force-space for the normal-tangential plane. The frictional adhesion model has been fitted to the data showing reasonable agreement between ideal model and DPS data over the normally used range of forces. DPS vary from idealized frictional adhesion model as adhesion forces eventually saturate with increasing tangential forces. Best-fit of the frictional adhesion model to the data yielded the following parameter values: $\mu \approx 0.5$, $\alpha^* \approx 25°$ and $F_{\max} \approx 1.0$ N.
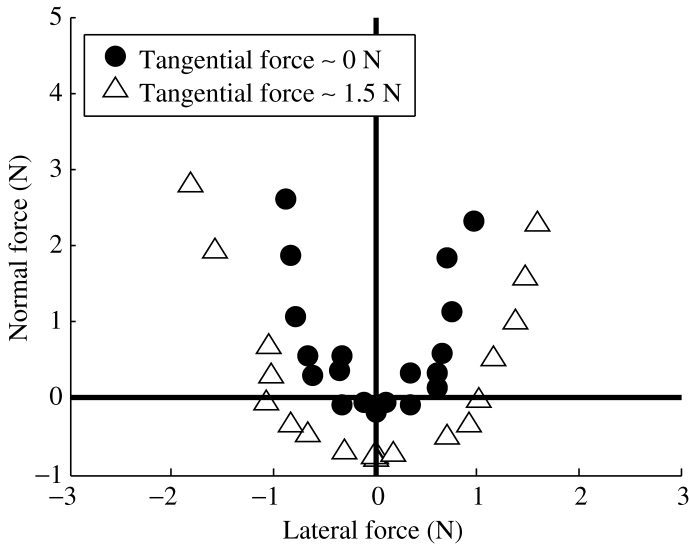
Figure 11. Contact failure forces (shown as circles and triangles in the figure) of the 3.9 cm² DPS patches in force–space for the normal–lateral plane for two different values of applied tangential force. Data show a behavior similar to that predicted by the JKR model. When adhesion is initially present due to an applied tangential force, increasing the lateral forces will decrease and eventually eliminate the amount of sustainable adhesion.

sliding, in the case of positive normal forces. The frictional adhesion model has been fitted to the data, resulting in $\mu \approx 0.5$, $\alpha^* \approx 25°$ and $F_{max} \approx 1.0$ N for the model parameters. Clearly, the data do not behave exactly as the model; however, there are some striking similarities. The data from the DPS are directional, like the model, only exhibiting adhesion when loaded with the angle of the stalks. The data appear to intersect the origin, exhibit Coulomb friction when pulled against the preferred adhesive direction, and show adhesion proportional to the applied tangential load up to a limit. The DPS data begin to look less like the frictional adhesion model as higher shear load is applied. Eventually, adhesion begins to saturate and there is no sharp limit as in the ideal frictional adhesion model. It should be noted that the data in Fig. 10 also resemble the Kendall peel model [8]. However, the Kendall peel model does not intersect the origin and the DPS data before saturation follow a more linear pattern than the Kendall peel model. The correspondence is not surprising, given that each individual stalk peels in a fashion similar to a tapered, elastic piece of tape.

Figure 11 shows data in the normal-lateral plane. Results are shown for two different values of tangential force. The adhesive behavior of the DPS in the lateral direction is, not surprisingly, symmetric since the stalks are also symmetric in the lateral direction. Comparing the results with Fig. 2, we observe that behavior is similar to that of the JKR model for a spherical contact against a flat substrate. When adhesion is initially present because some tangential load has been applied,
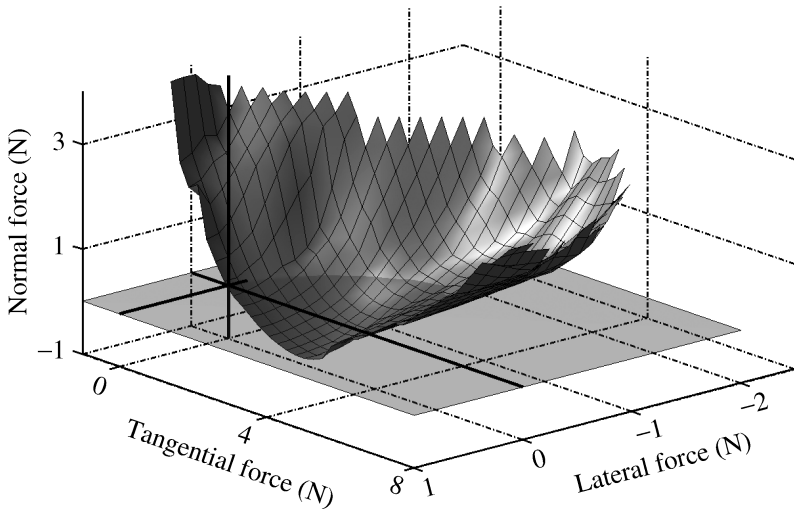
Figure 12. 3D limit surface of the DPS patches. Only half of the limit surface is shown for clarity, but the data are roughly symmetrical about the normal–tangential plane. Limit surface is constructed by piecewise linear interpolation of the normal, tangential and lateral forces measured at contact failure. Data used for linear interpolation were gathered from a large set of different pulloff trajectories. Surface is bowl-shaped and anisotropic in the tangential direction.

lateral loads decrease the amount of adhesion until eventually adhesion is eliminated and friction is observed.

The data in Figs 10 and 11 are essentially 'slices' of what is really a 3-dimensional convex surface. Such a surface is referred to as the limit surface [30] of a contact and describes the maximum values of force in 3-dimensional space that can be applied before the contact fails either because the surfaces pull apart from or begin to slide on one another. Figure 12 shows what the limit surface for the DPS looks like (only one half is shown for clarity; however, the data were roughly symmetric about the normal-tangential plane). The surface shown is generated *via* linear interpolation of data gathered from a large set of pulloff angles in three dimensions. The surface is clearly anisotropic in the tangential direction and is somewhat bowl-shaped. Combinations of normal, tangential and lateral forces that lie within the convex surface can be sustained by the contact; forces outside the convex surface will cause detachment or sliding. The limit surface can be used in planning and controlling safe contact forces to be exerted at the feet of a climbing robot.

4.2.5. Future tests. Further tests are planned to explore the behavior of these synthetic directional adhesives. DPS patches have been primarily tested on glass substrates and it is not fully known how surface roughness will affect adhesion performance. An initial test of the DPS on machined granite showed a 60% decrease in adhesion when compared to glass. The average roughness (R_a, average height of surface asperities) of the machined granite is ≈ 10 μm and the average roughness of glass is < 10 nm.

When moving to three dimensions, the parameter space becomes much larger. In all tests, the approach trajectory was held constant at 45° and speed was maintained at 1 mm/s to avoid dynamic effects. Changes in the approach trajectory and speed may also affect results.

4.3. Application to a climbing robot

The ultimate purpose of the DPS and the work presented here is to emulate the climbing ability of the gecko. The DPS were applied to a climbing robot platform named StickyBot [32]. StickyBot is a 4-legged robot actuated with servomotors and equipped with some force sensing capabilities in its limbs. Each foot of StickyBot has 4 toes and each toe of StickyBot is equipped with one elliptical-shaped patch of DPS, resulting in an upper bound of 15.6 cm^2 per foot (in practice the area is smaller, as the proximal regions do not fully contact the substrate; on average, approximately only 75% of the DPS stalks engage the surface with each foot placement). More detailed information on the design and control of StickyBot can be found in [32].

Initial attempts to climb used flat, unstructured sticky materials such as Sorbothane^{TM} (Sorbothane, Kent, OH, USA) and various polyurethanes. StickyBot is equipped with a peeling mechanism and it was intended that these adhesives would be peeled away from the surface similar to the Kendall tape peel model. However, these attempts failed to reproduce reliable and smooth climbing because the adhesion was not controllable. Large forces were required to both attach these adhesives and to peel them from the surface. At the moment that the toes would finally 'pop' off the surface, sudden force discontinuities at the contact produced vibrations that often caused other feet to slip. In addition, the amount of time that it took to peel these adhesives from the surface severely limited the overall speed at which StickyBot could climb.

With the use of DPS patches instead of unstructured, non-directional sticky materials, StickyBot has demonstrated climbing at speeds of 6 cm/s. StickyBot is able to load and unload its feet without high normal preload or pulloff forces and still sustain the required adhesion and tangential forces during stance. Figure 13 shows a comparison of the forces at one of StickyBot's feet during an attach/load/detach cycle using both an unstructured, non-directional adhesive and the DPS patches. The unstructured patch requires larger amounts of preload to initially attach to the surface and requires much larger forces at detachment. The DPS patches show little to no adhesion force at detachment, since, to detach, StickyBot simply unloads the tangential force at that foot by pulling against the stalk angles. The directionality of the DPS allows StickyBot to control the adhesion and climb smoothly and robustly.

5. CONCLUSIONS AND FUTURE WORK

An evaluation of current gecko inspired adhesive research shows that no synthetic material has replicated all of the desirable properties of the gecko's adhesive system.
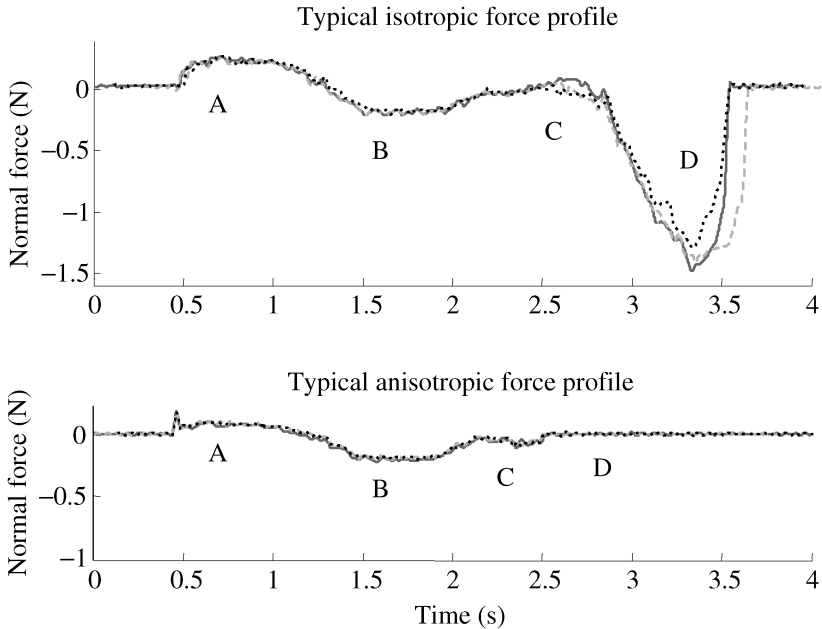
Figure 13. Comparison of force profiles of one foot of StickyBot through an attach/load/detach cycle using both a flat, unstructured isotropic adhesive patch and the directional, anisotropic DPS patches. The isotropic patches required higher preloads at attachment (A) to generate the same amount of adhesion during stance (B) as the DPS patches. Isotropic patches required more time and generated much higher forces during unloading (C) and detachment (D). Three successive trials are given to show cycle to cycle variability.

Moreover, when we consider the characteristics that are most useful for climbing, many of the current synthetic adhesives are not suitable, despite having high levels of adhesion. In particular, we argue that directionality is the most important characteristic of a climbing robot adhesive because it allows the robot to control its adhesion through specific leg/foot trajectories. The manufacture of a directional adhesive (DPS) was described in detail and shown to yield significant improvements in climbing performance over a conventional isotropic adhesive. Investigation into the effects of varying the geometry of the directional adhesive is ongoing. Looking forward, the next sequentially important traits of a climbing robot adhesive are small feature size and hierarchical compliance, which together will expand the range of climbable surfaces and lead to more robust overall performance.

Several methods of scaling down the DPS design are currently being explored. A 4× size reduction is possible through the use of a miniature precision mill and custom tooling. While this advance will likely improve the performance of the climbing robot, microfabrication methods provide an opportunity to scale DPS stalks to only a few micrometers in diameter, a reduction of almost 100 times. Unfortunately, most MEMS and nanofabrication methods are lithographic and are essentially $2\frac{1}{2}$-dimensional. That is, complex geometries can be created

(a)   (b)
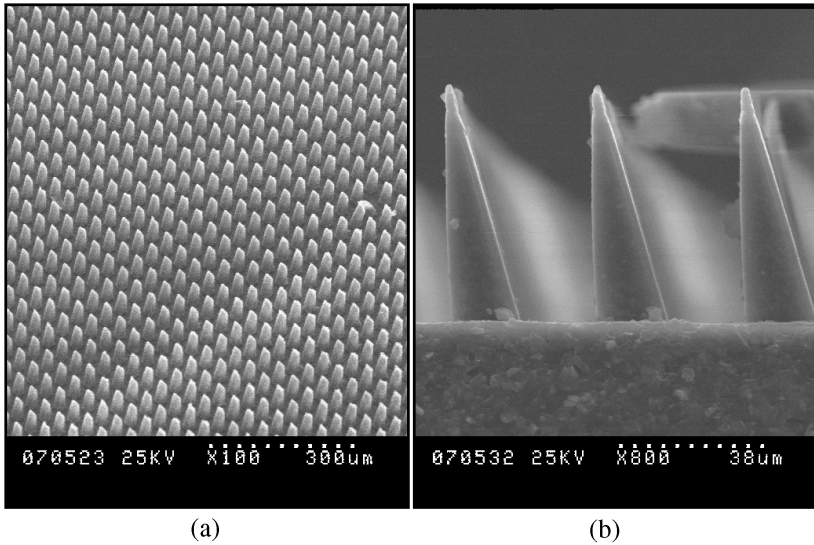
Figure 14. MicroDPS made of PDMS manufactured using a two exposure angle lithographic process to create a mold from SU-8 photoresist. (a) Stalks shown are 20 μm square posts, oriented vertically with an angled face. (b) Side view closeup of stalks. These stalks show adhesion comparable to the original DPS but require somewhat higher preloads. Stiffer materials are currently being investigated in order to create microDPS with improved durability and resistance to dirt.

in the horizontal plane, but vertical geometries are limited and subject to 'stair stepping'. However, a lithographic process has been developed that utilizes two exposure angles (90° and 24°) to create a mold from negative tone SU-8 photoresist (MicroChem, Newton, MA, USA), which can be spun to ≈300 μm thickness. The SU-8 is hard baked and used to shape soft PDMS elastomer into microDPS arrays under vacuum. The latest versions of these new microDPS show promising results (Fig. 14). Adhesion levels are comparable to the original DPS; however, the new microstructures require somewhat higher preloads. The microDPS are being manufactured from stiffer materials, which should result in increased flaw tolerance, durability, and resistance to fouling. Occasional failures in the DPS, such as the tip curling shown in Fig. 15, should become less frequent, leading to a longer service life (we note, however, that some of the original DPS patches have survived for over 6 months of use). The authors invite discussions from specialists in micro- and nano-fabrication processes concerning approaches that will permit the creation of three-dimensional, angled and contoured structures to match the directional behavior of the gecko setae.

In parallel, ongoing work aims to incorporate hierarchical compliance into the next generation climbing robot adhesives. The three main stages of compliance being considered are the lamellar scale (mm), setal scale (μm), and spatular scale (nm). Combining two or three of these length scales in an adhesive will allow the structures to conform to micro-rough surfaces such as frosted glass or flat interior wall paint. The addition of larger compliant features will also
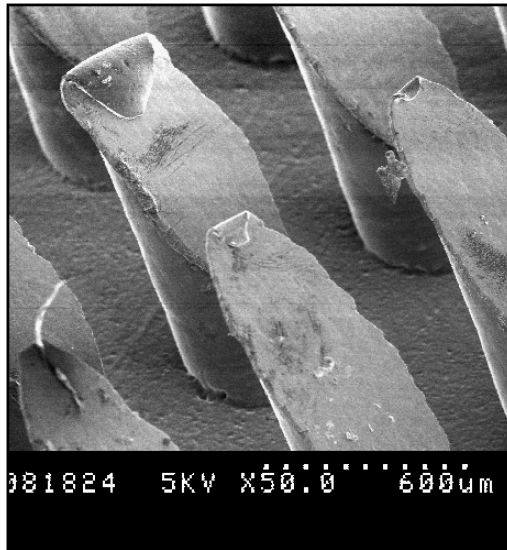
Figure 15. Example of a self-stick failure in current DPS. Tips of the DPS curl over and stick to the angled face, which reduces the overall adhesion of the DPS patches.

help to prevent the formation of local stress concentrations that initiate premature peeling. Two prototypes of hierarchical structures are shown in Fig. 16, one combining lamellae and setae sized features and the other combining setae and spatulae sized components. The integration of such components presents novel fabrication challenges because they are typically produced using entirely different processes. For example, the processes used to create aligned arrays of multi-wall carbon nanotubes would destroy most polymeric arrays. Consequently, the structure shown in Fig. 16 was created by bonding a patterned array of vertically aligned nanotubes to a prefabricated array of polymer stalks, encased in a temporary matrix of sacrificial material. As seen in the SEM image, the bonding process was quite imperfect.

While many efforts are being made to improve the performance and production of synthetic dry adhesives, much fundamental work remains. Accurate models of the contact stresses that angled stalks and tips experience when subjected to three-dimensional load trajectories like those suggested by the frictional adhesion model have yet to be developed. These would be very helpful in designing more optimized DPS shapes and sizes. The analysis is complicated by the very large strains and viscoelastic material properties involved. Additionally, understanding how the climbing forces are distributed, from the robot's weight and dynamics, through the legs and multiple stages of hierarchical compliance, to the contacts, is critical in designing a system that climbs without failures. From the standpoint of robotics, sensors are needed to determine when a strong contact has been achieved and when a contact is on the verge of failing, so that the robot can take preventative action. As these challenges are met, the performance of climbing robots like StickyBot will
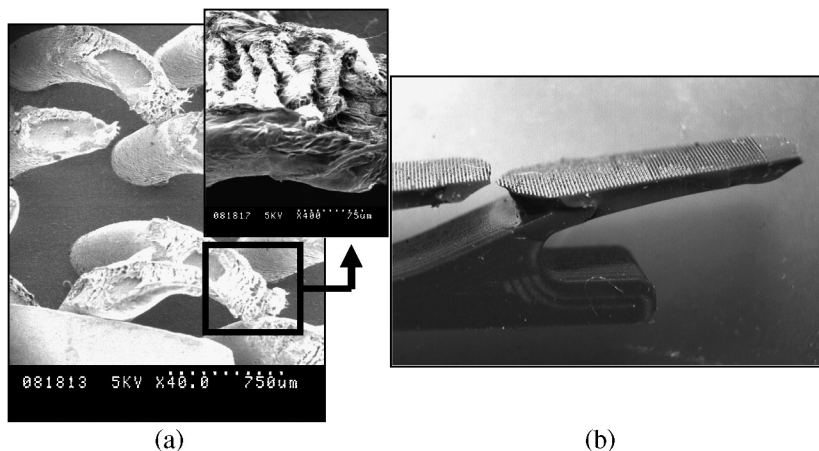
Figure 16. Hierarchical adhesive structures. (a) Combination of multi-wall carbon nanotubes with DPS, a two-stage structure similar to the gecko's setae/spatulae system. (b) Combination of PDMS flaps with microDPS, a two-stage structure similar to the gecko's lamellae/setae system.

continue to improve, eventually leading the transfer of technology from light and fragile test platforms to payload-bearing robots useful for sensing and exploration in dangerous environments.

Acknowledgements

REFERENCES

1. K. Autumn, S. T. Hsieh, D. M. Dudek, J. Chen, C. Chitaphan and R. J. Full, *J. Expl. Biol.* **209**, 260–272 (2006).
2. K. Autumn, in: *Biological Adhesives*, A. Smith and J. Callow (Eds), pp. 225–256. Springer, Berlin (2006).
3. T. Kim and B. Bhushan, *J. Adhesion Sci. Technol.* **21**, 1–20 (2007).
4. K. Autumn, Y. A. Liang, S. T. Hsieh, W. Zesch, W.-P. Chan, W. Kenny, R. Fearing and R. Full, *Nature* **405**, 681–685 (2000).
5. K. Autumn and A. Peattie, *Integr. Comp. Biol.* **42**, 1081–1090 (2002).
6. K. Autumn, A. Dittmore, D. Santos, M. Spenko and M. Cutkosky, *J. Expl. Biol.* **209**, 3569–3579 (2006).
7. K. Johnson, K. Kendall and A. Roberts, *Proc. R. Soc. Lond. A* **324**, 301–313 (1971).
8. K. Kendall, *J. Phys. D: Appl. Phys.* **8**, 1449–1452 (1975).
9. D. Campolo, S. Jones and R. Fearing, in: *Proc. of the 3rd IEEE Conference on Nanotechnology*, pp. 856–859, San Francisco, CA (2003).
10. A. Geim, S. Dubonos, I. Grigorieva, K. Novoselov, A. Zhukov and S. Shapoval, *Nature Materials* **2**, 461–463 (2003).

11. S. Gorb, M. Varenberg, A. Peressadko and J. Tuma, *J. R. Soc. Interface* **4**, 271–275 (2007).
12. H. Jeong, S. Lee, P. Kim and K. Suh, *Nano Lett.* **6**, 1508–1513 (2006).
13. D. Kim, H. Lee, J. Lee, S. Kim, K.-H. Lee, W. Moon and T. Kwon, *Microsyst. Technol.* **13**, 601–606 (2007).
14. S. Kim and M. Sitti, *Appl. Phys. Lett.* **89**, 261911 (2006).
15. M. Northen and K. Turner, *Sensors and Actuators A* **130**, 583–587 (2006).
16. A. Peressadko and S. Gorb, *J. Adhesion* **80**, 247–261 (2004).
17. M. Sitti and R. Fearing, *J. Adhesion Sci. Technol.* **17**, 1055–1073 (2003).
18. B. Yurdumakan, R. Raravikar, P. Ajayanb and A. Dhinojwala, *Chem. Commun.* **30**, 3799–3801 (2005).
19. Y. Zhao, T. Tong, L. Delzeit, A. Kashani, M. Meyyapan and A. Majumdar, *J. Vac. Sci. Technol. B* **24**, 331–335 (2006).
20. K. Daltorio, S. Gorb, A. Peressadko, A. Horchler, R. Ritzmann and R. Quinn, in: *Proc. of the 8th International Conference on Climbing and Walking Robots*, pp. 131–138, London (2005).
21. O. Unver, A. Uneri, A. Aydemir and M. Sitti, in: *Proc. of the IEEE International Conference on Robotics and Automation*, pp. 2329–2335, Orlando, FL (2006).
22. K. Autumn, C. Majidi, R. E. Groff, A. Dittmore and R. Fearing, *J. Expl. Biol.* **209**, 3558–3568 (2006).
23. C. Dahlquist, in: *Treatise on Adhesion and Adhesives*, R. L. Patrick (Ed.), Vol. 2, pp. 219–260. Marcel Dekker, New York (1969).
24. H. Gao, X. Wang, H. Yao, S. Gorb and E. Arzt, *Mech. Mater.* **37**, 275–285 (2005).
25. B. Bhushan and R. Sayer, *Microsyst. Technol.* **13**, 71–78 (2007).
26. M. Northen and K. Turner, *Nanotechnology* **16**, 1159–1166 (2005).
27. M. Northen, K. Turner, C. Greiner and E. Arzt, in: *Proc. of the Solid-State Sensors, Actuators, and Microsystems Workshop*, pp. 43–46, Hilton Head Island, SC (2006).
28. B. Aksak, M. P. Murphy and M. Sitti, *Langmuir* **23**, 3322–3332 (2007).
29. K. Daltorio, A. Horchler, S. Gorb, R. Ritzmann and R. Quinn, in: *Proc. of the International Conference on Intelligent Robots and Systems*, pp. 3648–3653, Alberta, Canada (2005).
30. S. Goyal, A. Ruina and J. Papadopoulos, in: *Proc. of the IEEE International Conference on Robotics and Automation*, pp. 794–799, Scottsdale, AZ (1989).
31. A. Crosby, M. Hageman and A. Duncan, *Langmuir* **21**, 11738–11743 (2005).
32. S. Kim, M. Spenko, S. Trujillo, B. Heyneman, V. Matolli and M. Cutkosky, in: *Proc. of the IEEE International Conference on Robotics and Automation*, pp. 1268–1273, Rome, Italy (2007).